

20. N. Cotte *et al.*, *Geophys. J. Int.* **138**, 809 (1999).  
 21. W. Friederich, *Geophys. J. Int.* **153**, 88 (2003).  
 22. Z. Huang, W. Su, Y. Peng, Y. Zheng, H. Li, *J. Geophys. Res.* **108**, 2073 (2003).  
 23. R. Rapine, F. Tilmann, M. West, J. Ni, A. Rodgers, *J. Geophys. Res.* **108**, 2120 (2003).  
 24. H. F. Sherrington, G. Zandt, A. Frederiksen, *J. Geophys. Res.* **109**, B02312 (2004).  
 25. N.M. Shapiro, V. Levin, M.H. Ritzwoller, P. Molnar, D. Smith, *Eos* **84** (no. 46) (suppl.), F985 (abstr. S11C-0307) (2003).  
 26. T. Weiss, S. Siegesmund, W. Rabbel, T. Bohlen, M. Pohl, *Pure Appl. Geophys.* **156**, 97 (1999).  
 27. O. Nishizawa, T. Yoshitno, *Geophys. J. Int.* **145**, 19 (2001).  
 28. A. Meltzer, N. Christensen, *Geophys. Res. Lett.* **28**, 2129 (2001).  
 29. K. S. Aleksandrov, T. V. Ryzhova, *Izv. Akad. Nauk SSSR Ser. Geofiz.* **12**, 186 (1961).  
 30. M. Barazangi, J. Ni, *Geology* **10**, 179 (1982).  
 31. P. Molnar, P. England, J. Martinod, *Rev. Geophys.* **31**, 357 (1993).  
 32. We used the central moment tensor catalog available on the Harvard Web site: [www.seismology.harvard.edu/CMTsearch.html](http://www.seismology.harvard.edu/CMTsearch.html).  
 33. Details of the computations are presented on *Science Online*.  
 34. K. D. Nelson *et al.*, *Science* **274**, 1684 (1996).  
 35. Y. Makovsky, S. L. Klemperer, *J. Geophys. Res.* **104**, 10795 (1999).  
 36. S. Roecker, *Eos* **80** (no. 46) (suppl.), F1017 (abstr. T41C-14) (1999).  
 37. A. F. Sheehan *et al.* *Eos* **80** (no. 47) (suppl.), F994 (abstr. S61D-11) (2002).  
 38. Most of the data used in this work were obtained from the Incorporated Research Institution for Seismology

Data Management Center and the GEOSCOPE Data Center. We are also particularly grateful to J. Trampert at Utrecht University; M. Antolik, A. Dziewonski, and G. Ekström at Harvard University for providing phase speed measurements; A. Sheehan and F. Wu for providing the HIMNT data; A. Levshin and A. van Hunen for help in preparing the data set; and P. England and C. Jones for helpful discussions. This work was supported by NSF grant EAR-0337622.

**Supporting Online Material**

[www.sciencemag.org/cgi/content/full/305/5681/233/DC1](http://www.sciencemag.org/cgi/content/full/305/5681/233/DC1)

Materials and Methods  
Figs. S1 to S3

24 March 2004; accepted 1 June 2004

# InSAR Observations of Low Slip Rates on the Major Faults of Western Tibet

Tim J. Wright,<sup>1\*</sup> Barry Parsons,<sup>1</sup> Philip C. England,<sup>1</sup> Eric J. Fielding<sup>2</sup>

Two contrasting views of the active deformation of Asia dominate the debate about how continents deform: (i) The deformation is primarily localized on major faults separating crustal blocks or (ii) deformation is distributed throughout the continental lithosphere. In the first model, western Tibet is being extruded eastward between the major faults bounding the region. Surface displacement measurements across the western Tibetan plateau using satellite radar interferometry (InSAR) indicate that slip rates on the Karakoram and Altyn Tagh faults are lower than would be expected for the extrusion model and suggest a significant amount of internal deformation in Tibet.

Western Tibet lies between the Indian plate and the Tarim Basin (Fig. 1), an undeforming block whose motion relative to Eurasia is mainly taken up by deformation in the Tien Shan range to the north (1). The two major strike-slip faults of the region are the Karakoram Fault, running NW-SE in the southern part of the plateau; and the western end of the Altyn Tagh Fault system, which runs approximately E-W at the northern end of the region. Models that regard India's motion relative to Tarim as being taken up principally by eastward extrusion on these strike-slip faults postulate about 30 mm/year of dextral (right-lateral) slip on the Karakoram Fault, and 20 mm/year of sinistral (left-lateral) slip on the western Altyn Tagh (2–5). In contrast, models that consider the continental lithosphere to resemble continuous media, with faults representing the near-surface localization of distributed deformation at depth (6–

8), predict eastward extrusion of Tibet at no more than about 10 mm/year (8–10)

Previous measures of the rate of slip on these major fault systems have come from the offsets of geologic features, divided by the estimated ages of those features, and from geodetic measurements of recent (less than 10 years) ground displacement on lines crossing the faults. Offsets of up to ~1000 km have been reported for geologic markers along the Karakoram Fault (3); division of such offsets by the presumed 30-million-year age of the motion yields a rate of ~30 mm/year, consistent with the rate of  $32 \pm 8$  mm/year calculated by dividing the observed

offsets of glacial moraine deposits by a presumed age of ~10,000 years (11). However, lower rates of 4 to 8 mm/year, based on geologic observations, have also been proposed for the Karakoram Fault (12, 13). These lower rates agree with geodetic measurements made over the past 10 years, which suggest rates of  $3 \pm 5$  mm/year (14) and  $11 \pm 4$  mm/year (15).

On the Altyn Tagh Fault system, geologic estimates of slip rates are generally about 30 mm/year along the main portion of the Altyn Tagh Fault, with a somewhat lower rate (~20 mm/year) at the western end (16). In contrast, geodetic measurements yield estimates of the rate of slip on the Altyn Tagh Fault system of ~10 mm/year in its main portion (1, 17, 18) and  $7 \pm 3$  mm/year in its western portion (1).

Attempts to explain the discrepancies between different studies include the suggestions that the ages assumed for offset glacial features may be underestimated by a factor of 3 or more (12, 19) and that field-based measurements, whether geologic or geodetic, may underestimate the total displacement across strike-slip zones. Satellite radar interferometry (InSAR) can circumvent these difficulties by producing maps of crustal deformation, with a spatial resolution of a few tens of meters and a precision of a few millimeters, that cover regions hundreds of kilometers in extent. Although measuring interseismic deformation is difficult using InSAR because of the small deformation signal, a few studies have shown that it is possible, provided that

**Table 1.** Interferograms (ifm's) used in this study.

	Image 1*	Image 2	Time interval	$B_{\perp}$ (m)†	$\sigma$ (mm/year)‡
ifm1	13 November 1992 (ERS-1)	24 June 1996 (ERS-2)	3.6 years	-30 to 26	1.7
ifm2	11 June 1993 (ERS-1)	7 October 1996 (ERS-2)	3.3 years	-17 to -90	1.2
ifm3	3 December 1993 (ERS-1)	22 October 1995 (ERS-1)	1.9 years	-31 to 77	1.8
ifm4	15 April 1996 (ERS-1)	4 April 1999 (ERS-1)	3.0 years	24 to 10	1.4
ifm5	19 May 1996 (ERS-1)	5 April 1999 (ERS-2)	2.9 years	68 to 91	2.0

\*SAR data (from the European Space Agency) are from standard descending track 291, frames 2871 to 2943. Individual interferograms are shown in fig. S1. † $B_{\perp}$  is the perpendicular baseline separation of the satellite orbits at the scene center and varies along the track between the values shown. ‡Standard deviation of the interferogram noise on the plateau.

<sup>1</sup>COMET, Department of Earth Sciences, University of Oxford, Oxford, UK. <sup>2</sup>Jet Propulsion Laboratory, California Institute of Technology, Pasadena, CA 91109, USA, and Department of Earth Sciences, University of Cambridge, UK.

\*To whom correspondence should be addressed. E-mail: [tim.wright@earth.ox.ac.uk](mailto:tim.wright@earth.ox.ac.uk)

multiple interferograms are used (20, 21). We exploited this capability to map the deformation of western Tibet and to estimate the total slip rate for each of its major fault systems.

We used 500-km-long strips of radar data acquired by the ERS-1 and ERS-2 satellites between 1992 and 1999. These data span the

entire width of the western plateau, from the Tarim basin in the north to just north of the Himalayas, where the slopes are too steep for displacements to be obtained with ERS InSAR (Fig. 1). The five independent interferograms produced cover time intervals of 1.9 to 3.6 years (Table 1). The topographic phase contri-

bution was removed using a 3-arc-sec (~90-m) digital elevation model from the Shuttle Radar Topography Mission (SRTM) (22). The interferograms were summed and divided by the total time interval, 14.7 years, to determine the mean yearly range change (Fig. 2A). The lack of vegetation on the high Tibetan plateau allows a coherent signal over much of the ground area, even in our longer-interval interferograms (figs. S1 and S2), except in the areas of highest elevation, where we lose coherence in some interferograms, probably due to snow cover.

The biggest sources of uncertainty in InSAR data arise from differences in atmospheric water vapor between scenes, from errors in satellite orbits, and from errors in the surface elevations used to correct the topographic phase contribution (23). At lower surface elevations, water vapor is the most problematic source of error for InSAR data. Over the 5000-m-high Tibetan plateau, however, the total amount of water vapor above the surface is low. We estimate a  $1\sigma$  error in mean yearly phase change of 0.7 mm/year on the plateau, rising to 1.8 mm/year at the northern end of the region, where the elevation drops by about 3000 m into the Tarim basin (Fig. 3 and supporting text).

InSAR observations (range changes) measure the component of deformation in the satellite line of sight, which is  $23^\circ$  from vertical at the swath center and perpendicular to the satellite flight direction. Thus, the interferograms (Fig. 2) are most sensitive to horizontal motion in a direction  $N78^\circ W$ , which is roughly parallel to the two major strike-slip faults. For example, a left-lateral slip rate of 20 mm/year on faults parallel to the western Allyn Tagh Fault, almost perpendicular to the satellite track, would give a positive range change of around 7 mm/year north of the fault with respect to the south; and a 30 mm/year right-lateral slip rate on the Karakoram Fault, which is slightly less favorably oriented with respect to the flight direction, would result in a range change of nearly 8 mm/year (north side negative).

Our interferograms are also sensitive to any relative vertical motions across the fault zones, which could cause range changes in an opposite sense to the horizontal motions. However, topographic profiles across the Karakoram Fault in the area of our interferograms (Fig. 3B) suggest that there is no long-term relative vertical motion across it. Although there is geologic evidence for thrust faulting around 100 km north of the Allyn Tagh Fault at the edge of the Tarim Basin (24), Global Positioning System (GPS) data (1) suggest that the present-day rate of convergence here is less than 4 mm/year (Fig. 1). Furthermore, this deformation would cause range changes that are spatially distinct from those caused by strike-slip motion on the Allyn Tagh Fault. We therefore assume that horizontal motion is dominant.

We determined the maximum interseismic slip rates for the Karakoram and Allyn Tagh

**Fig. 1.** Tectonic and topographic map of western Tibet. The blue rectangle delimits the extents of our SAR data, acquired on standard ERS descending track 291. Surface topography is from the GTOPO30 1-km digital elevation model; red lines show major faults, and GPS velocities relative to Eurasia (1, 32) are given as white arrows, with 95% confidence limits marked by the ellipses. The dashed black box shows the extent of Fig. 2. LGC, Longmu Gozha Co Fault.

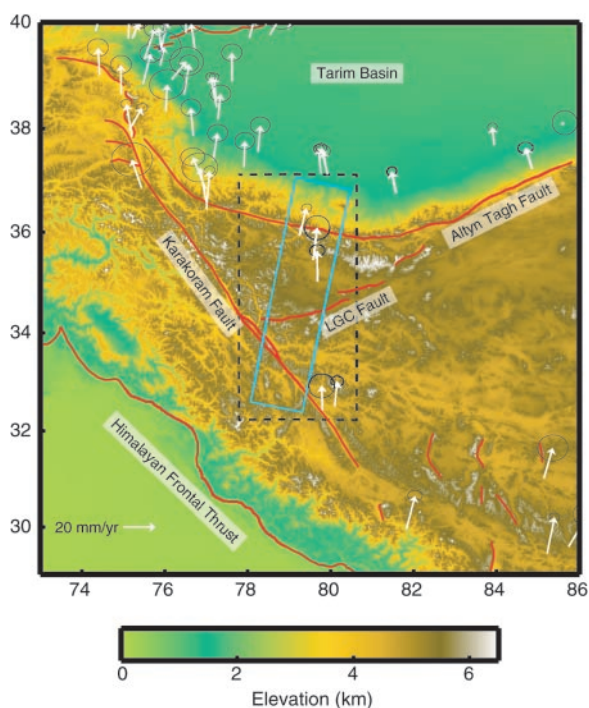
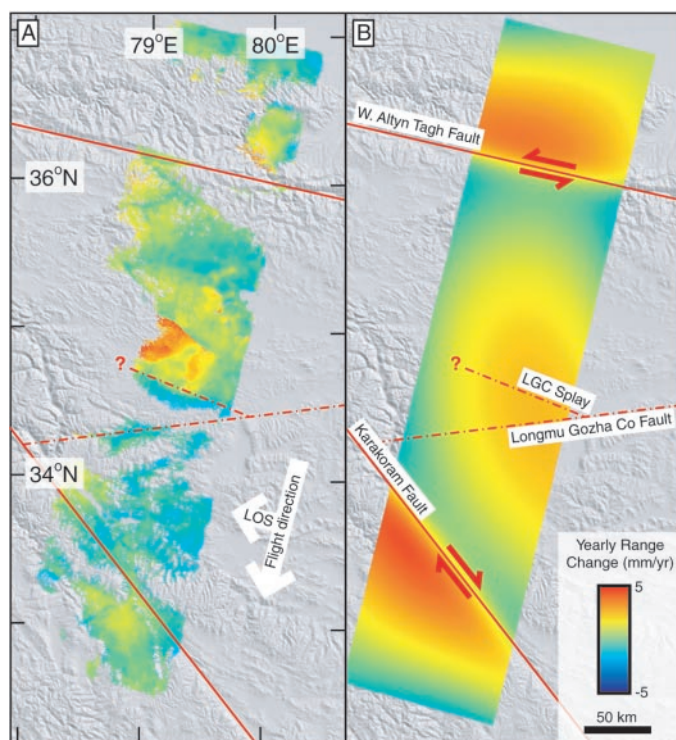


**Fig. 2.** (A) Mean observed yearly range change: the sum of the interferograms that are coherent for a given pixel (if there are at least three) divided by their total time interval. Red indicates increases in range [motion away from the satellite, whose flight direction and line of sight (LOS) are given] and blue indicates range decreases. (B) Synthetic interferogram generated by projecting the predictions of a simple elastic dislocation model, in which the Karakoram Fault slips at 30 mm/year and the Allyn Tagh at 20 mm/year, below a 10-km elastic lid into the satellite line of sight, and removing a quadratic phase ramp, to simulate the effect of the orbital baseline adjustment (fig. S2). The strong localized signals on the Allyn Tagh and Karakoram Faults are absent in the real data. Shaded relief from SRTM topography data (22) is shown in the background.



Faults that are consistent with the InSAR data. We use a model in which faults are assumed to slip aseismically at depth underneath a locked elastic lid. Surface displacements are then equivalent to those caused by an infinitely long screw dislocation in an elastic half-space (25). We use a 10-km locking depth [consistent with the rupture extent in the 1997 Manyi earthquake (26) and graben flank uplift observations (27)] and slip rates of 30 mm/year and 20 mm/year on the Karakoram and Altyn Tagh faults, respectively. The predicted surface displacements are then projected onto the local line-of-sight vector to the satellite and show strong range changes associated with both faults. Localized range changes remain even when applying the orbital correction to this model interferogram (Fig. 2B and fig. S3). We also constructed profiles of range change in the individual and stacked interferograms along the entire length of the interferogram, as well as perpendicular to the Karakoram and western Altyn Tagh Faults, by averaging all the phase data perpendicular to the profile in 10-km bins along it, to compare with model predictions (Fig. 3).

For the Karakoram Fault Zone, the observed range changes across the fault are much smaller than those required by models with slip rates of 30 mm/year. To determine a range of acceptable slip rates, we held the locking depth fixed at 10 km and solved for the best-fit slip rate in a least-squares sense. Best-fit quadratic ramps to the InSAR data were also determined to allow for the effects of incorrectly modeled orbital phase. Tests show (supporting text) that this procedure is able to recover the correct model slip rates for inversions of synthetic data that had been subjected to such orbital adjustments. To account for data uncertainties, we used a Monte Carlo simulation technique in which correlated noise, with the same characteristics as that in the real interferograms, was simulated and added to the original data sets (28). The inversion of these perturbed data sets yielded an ensemble of model slip rate solutions, the distribution of which gave the uncertainties. The right-lateral slip rate of the Karakoram Fault was found to be in the range of  $1 \pm 3$  mm/year, corresponding to an upper bound of 7 mm/year at the 95% confidence level; the

left-lateral slip rate of the Altyn Tagh Fault was found to be  $5 \pm 5$  mm/year. Inversions in which the locking depth was increased to 15 km did not change the best-fit slip rates but increased the uncertainties slightly to 4 mm/year and 6 mm/year for the Karakoram and Altyn Tagh Faults, respectively.

Because our data span western Tibet, we are able to investigate the deformation across less prominent faults within the plateau. There is a strong phase signature associated with a possible splay of the Longmu Gozha Co Fault (Fig. 2), consistent with  $\sim 10$  mm/year left-lateral strike-slip motion across it (fig. S4D), or alternatively around 5 mm/year of dip-slip motion (north down). By contrast, the Longmu Gozha Co Fault itself does not appear to be accumulating any left-lateral strain at present (fig. S4C). It is also possible that other, nontectonic deformation sources are present in this area: The range changes in the individual interferograms are quite variable here (fig. S2), which suggests possible seasonal effects.

Our upper limit of 7 mm/year for the right-lateral slip rate on the Karakoram Fault is smaller than the rate postulated by extrusion models (4, 5) but is consistent with recent geologic and geodetic estimates of relative motion across the fault (12, 14). Although further data are required to reduce the uncertainty due to atmospheric effects, the left-lateral slip rate of  $5 \pm 5$  mm/year on the western Altyn Tagh (Karakax) Fault is also smaller than the geologic estimate of 20 mm/year suggested by extrusion models (1, 16) but is close to the rate of  $7 \pm 3$  mm/year deduced from GPS measurements (1). A comparable conclusion may also be drawn for the central Altyn Tagh Fault, east of the section considered here, where a lower bound of slip rate ( $13 \pm 2$  mm/year) from geologic data (29) agrees with the GPS-determined rates of  $9 \pm 2$  mm/year (1, 17). Thus, dated geologic offsets and geodetic measurements yield consistent estimates of slip rate that are inconsistent with the rates postulated for the extrusion of western Tibet as a rigid body.

In addition, if Tibet were being extruded as a rigid body, then the left-lateral and right-lateral fault systems would each have to accommodate a comparable amount of eastward motion. Our observations rule out right-lateral motion of more than 7 mm/year on the Karakoram Fault and show no evidence for other major right-lateral faults in western Tibet; if the deformation associated with the possible splay to the Longmu Gozha Co Fault is indeed left-lateral strike-slip, there would be around 20 mm/year of left-lateral motion associated with the northern strike-slip faults in western Tibet. This difference in motion must represent the internal deformation of Tibet—an interpretation consistent with GPS data from eastern Tibet (30). We conclude that the InSAR data show the rates of internal de-

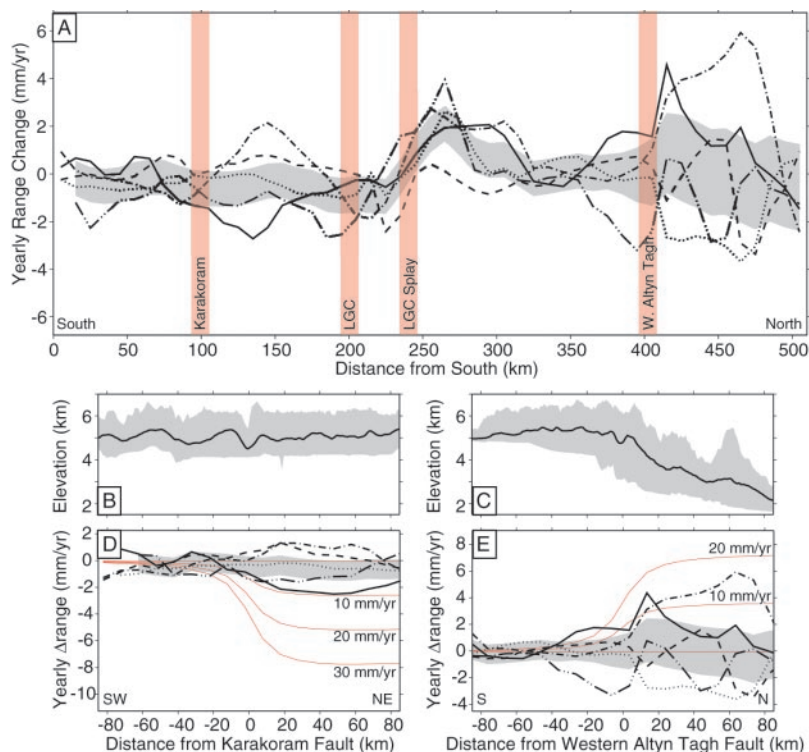


**Fig. 3.** (A) Profile, parallel to the SAR track, of yearly range changes averaged perpendicular to the profile in 10-km bins along it. The thick gray band is the mean yearly range change with its 1σ error bound (0.7 mm/year on the plateau, and 1.8 mm/year north of the Altyn Tagh Fault, with a 40-km transition centered on the fault). Individual interferograms (ifm's) (Table 1) are represented by the thick black lines (ifm1, solid; ifm2, dashes; ifm3, dash-dot; ifm4, dots; ifm5, dash-dot-dot-dash). The center of the swath crosses the labeled fault zones at the locations shown by the red bars. (B and C) Topographic profiles perpendicular to the Karakoram and western Altyn Tagh Faults. The black line is the mean elevation in 1-km bins along the profile, and the gray band shows the minimum and maximum elevations within the swath. (D and E) Yearly range change profiles perpendicular to the Karakoram and Altyn Tagh Faults. Symbols are as defined in (A). Red lines are profiles from synthetic interferograms with the same swath as the observed data, calculated using an elastic dislocation model in which pure strike-slip faults slip at the rates shown, under a 10-km elastic lid.

formation of the region (31) to be comparable with or larger than the rates of deformation associated with faults bounding western Tibet.

### References and Notes

- Z. K. Shen *et al.*, *J. Geophys. Res.* **106**, 30607 (2001).
- P. Tapponnier, G. Peltzer, R. Armijo, A.-Y. Le Dain, P. Cobbold, *Geology* **10**, 611 (1982).
- G. Peltzer, P. Tapponnier, *J. Geophys. Res.* **93**, 15085 (1988).
- J.-P. Avouac, P. Tapponnier, *Geophys. Res. Lett.* **20**, 895 (1993).
- P. Tapponnier *et al.*, *Science* **294**, 1671 (2001).
- P. Bird, K. Piper, *Phys. Earth Planet Inter.* **21**, 158 (1980).
- P. England, D. McKenzie, *Geophys. J. R. Astron. Soc.* **70**, 295 (1982).
- G. Houseman, P. England, *J. Geophys. Res.* **91**, 3651 (1986).
- G. Houseman, P. England, *J. Geophys. Res.* **98**, 12233 (1993).
- P. England, P. Molnar, *Nature* **344**, 140 (1990).
- Q. Liu, thesis, Université Paris (1993).
- E. T. Brown *et al.*, *J. Geophys. Res.* **107**, 2192 (2002).
- M. Searle, R. F. Weinberg, W. J. Dunlap, *Continental Transpressional and Transtensional Tectonics*, R. Holdsworth, R. Strachan, J. F. Dewey, Eds., *Geol. Soc. Spec. Pub.* **135**, 307 (1998).
- S. Jade *et al.*, *Geol. Soc. Am. Bull.*, in press.
- P. Banerjee, R. Bürgmann, *Geophys. Res. Lett.* **29**, 30 (2002).
- G. Peltzer, P. Tapponnier, R. Armijo, *Science* **246**, 1285 (1989).
- R. Bendick, R. Bilham, J. Freymueller, K. Larson, G. Yin, *Nature* **404**, 69 (2000).
- Z. Chen *et al.*, *J. Geophys. Res.* **105**, 16215 (2000).
- A. Gillespie, P. Molnar, *Rev. Geophys.* **33**, 311 (1995).
- T. J. Wright, B. E. Parsons, E. J. Fielding, *Geophys. Res. Lett.* **28**, 2117 (2001).
- G. Peltzer, F. Crampé, S. Hensley, P. Rosen, *Geology* **29**, 975 (2001).
- T. Farr, M. Koblrick, *Eos* **81**, 583 (2000).
- R. Hanssen, *Radar Interferometry: Data Interpretation and Error Analysis* (Kluwer Academic, Dordrecht, Netherlands, 2001).
- J.-P. Avouac, G. Peltzer, *J. Geophys. Res.* **98**, 21773 (1993).
- J. Savage, R. Burford, *J. Geophys. Res.* **78**, 832 (1973).
- G. Peltzer, F. Crampé, G. King, *Science* **286**, 272 (1999).
- J. Masek, B. Isacks, E. Fielding, *Tectonics* **13**, 659 (1994).
- T. J. Wright, Z. Lu, C. Wicks, *Geophys. Res. Lett.* **30**, 1974 (2003).
- A.-S. Meriaux *et al.*, *Geophys. Res. Abstr.* **5**, 08062 (2003).
- Z. Chen *et al.*, *J. Geophys. Res.* **109**, B01403 (2004).
- R. Armijo, P. Tapponnier, J. Mercier, T. Han, *J. Geophys. Res.* **91**, 13803 (1986).
- Q. Wang *et al.*, *Science* **294**, 574 (2001).
- Supported by the Natural Environment Research Council through the Centre for Observation and Modelling of Earthquakes and Tectonics as well as a research fellowship to T.J.W. We are grateful to the European Space Agency for providing the ERS SAR data used, and to NASA for the SRTM topography. Part of this research was performed at the Jet Propulsion Laboratory (JPL) under contract with NASA. We thank JPL/Caltech for the use of the ROLpac software to generate our interferograms and S. Lamb, R. Phillips, J. Jackson, and two anonymous reviewers for comments that have improved the manuscript. Some figures were prepared using the public-domain GMT software.

### Supporting Online Material

www.sciencemag.org/cgi/content/full/305/5681/236/DC1  
SOM Text  
Figs. S1 to S5  
References

3 February 2004; accepted 10 June 2004

## Derivatives of Erythropoietin That Are Tissue Protective But Not Erythropoietic

Marcel Leist,<sup>1\*</sup> Pietro Ghezzi,<sup>2,3\*</sup> Giovanni Grasso,<sup>3,4</sup>  
Roberto Bianchi,<sup>2</sup> Pia Villa,<sup>2,5</sup> Maddalena Fratelli,<sup>2</sup>  
Costanza Savino,<sup>2</sup> Marina Bianchi,<sup>2</sup> Jacob Nielsen,<sup>1</sup>  
Jens Gerwien,<sup>1</sup> Pekka Kallunki,<sup>1</sup> Anna Kirstine Larsen,<sup>1</sup>  
Lone Helboe,<sup>1</sup> Søren Christensen,<sup>1</sup> Lars O. Pedersen,<sup>1</sup>  
Mette Nielsen,<sup>1</sup> Lars Torup,<sup>1</sup> Thomas Sager,<sup>1</sup>  
Alessandra Sfacteria,<sup>3,4</sup> Serhat Erbayraktar,<sup>3,6</sup>  
Zubeyde Erbayraktar,<sup>3,6</sup> Necati Gokmen,<sup>6</sup> Osman Yilmaz,<sup>3,6</sup>  
Carla Cerami-Hand,<sup>3,7</sup> Qiao-wen Xie,<sup>3,7</sup> Thomas Coleman,<sup>3,7</sup>  
Anthony Cerami,<sup>3,7†</sup> Michael Brines<sup>3,7</sup>

Erythropoietin (EPO) is both hematopoietic and tissue protective, putatively through interaction with different receptors. We generated receptor subtype-selective ligands allowing the separation of EPO's bioactivities at the cellular level and in animals. Carbamylated EPO (CEPO) or certain EPO mutants did not bind to the classical EPO receptor (EPOR) and did not show any hematopoietic activity in human cell signaling assays or upon chronic dosing in different animal species. Nevertheless, CEPO and various nonhematopoietic mutants were cytoprotective in vitro and conferred neuroprotection against stroke, spinal cord compression, diabetic neuropathy, and experimental autoimmune encephalomyelitis at a potency and efficacy comparable to EPO.

Erythropoietin (EPO) is a pleiotropic cytokine originally identified for its role in erythropoiesis (1). Its hematopoietic effects on the bone marrow are mediated by the homodimeric erythropoietin receptor [(EPOR)<sub>2</sub>], a class 1 cytokine receptor. Sasaki and others identified the production of EPO in the central nervous system and, later, its neuroprotective function (1–7). Eventually, a proof-of-concept for neuroprotection by peripherally dosed EPO was obtained in a phase II clinical trial in cerebral ischemia (8).

Desialylated EPO (asialoEPO) has the same (EPOR)<sub>2</sub> affinity and neuroprotective properties as EPO, but an extremely short plasma half-life. Both molecules share the capacity of crossing an intact blood-brain barrier when dosed peripherally (3, 8–10), but bear also the risk of unwanted effects linked to the chronic overstimulation of (EPOR)<sub>2</sub>, for example, on the bone marrow.

Extensive structure-activity relationship (SAR) studies of EPO have identified regions and amino acids essential for binding to

(EPOR)<sub>2</sub> (11), and many chemical modifications that abolish EPO's hematopoietic bioactivity are known (12, 13). However, the receptor complex mediating the neuroprotective effects of EPO differs from the hematopoietic receptor with respect to apparent affinity for EPO, apparent molecular weight, and associated proteins (2). The EPO receptor has been reported to associate functionally with other cytokine receptors such as CD131 (14, 15), and a region of EPO not within the (EPOR)<sub>2</sub> binding domains has been associated with neuroprotective effects (16). On the basis of these observations, we postulated that molecular changes to erythropoietin that neutralize erythropoiesis would not necessarily alter tissue-protective potency. One known modification silencing erythropoiesis is the carbamylation of lysines, a process well recognized to profoundly alter protein conformation and function. Surprisingly, we found that carbamylated EPO is neuroprotective and therefore introduces a new class of neuroprotective cytokines that lack erythropoietic activity yet engage a tissue-protective receptor.

All lysines in EPO were transformed to homocitrulline by carbamylation (17) (fig. S1A). CEPO, the resultant product, completely lacked bioactivity in the in vitro UT7 hematopoiesis bioassay (Table 1) and failed to bind to EPOR on these cells (Fig. 1A). However,

<sup>1</sup>H. Lundbeck A/S, 2500 Valby, Denmark. <sup>2</sup>Mario Negri Institute of Pharmacological Research, 20157 Milano, Italy. <sup>3</sup>The Kenneth S. Warren Institute, Ossining, NY 10562, USA. <sup>4</sup>University of Messina, 98122 Messina, Italy. <sup>5</sup>Consiglio Nazionale delle Ricerche, Institute of Neuroscience, 20129 Milano, Italy. <sup>6</sup>Dokuz Eylul University School of Medicine, Izmir 35340, Turkey. <sup>7</sup>Warren Pharmaceuticals, Inc., Ossining, NY 10562, USA.

\*These authors contributed equally to this study.

†To whom correspondence should be addressed. E-mail: acerami@kswi.org